Pergamon

J. Mech. Phys. Solids, Vol. 43, No. 9, pp. 1409–1431, 1995

0022–5096/95 $9.50+0.00

0022–5096(95)00039–9

ON THE COLD COMPACTION OF POWDERS

N. A. FLECK

Cambridge University Engineering Department, Trumpington Street, Cambridge CB2 1PZ, U.K.

(*Received* 13 *August* 1994; *in revised form* 25 *March* 1995)

ABSTRACT

Constitutive models are developed for stage I cold compaction of powders under general loading. Densification is assumed to occur by plastic deformation at the isolated contacts between particles. The shape of the yield surface is found to be sensitive to the cohesive strength between particles and to be less sensitive to the degree of inter-particle friction. An internal state variable model is used to describe the evolution of anisotropy under general loading. The theory assumes that the distribution of contacts between particles can be approximated by a second order tensor **B**; a prescription is given for updating **B** as deformation proceeds. The predicted compaction behaviour for a state of uniaxial strain is in good agreement with experimental observations reported in the literature.

1. INTRODUCTION

The compaction of powders is a versatile fabrication route for monolithic metals, ceramics and polymers. Components can be made to net final shape from a wide range of alloy compositions. Particulate and fibre reinforced composites may also be manufactured with a powder matrix. At temperatures below about 0.3 of the absolute melting temperature, compaction is by low temperature plasticity; at higher temperatures power law creep and diffusional flow aid densification.

The initial packing density depends upon particle shape, particle size distribution and the degree to which the powder has been shaken down. For the case of dense random packing of monosized spheres the initial relative density is $D_0 = 0.64$, where the relative density D is the macroscopic density of the aggregate divided by the full density of the particulate material. The process of compaction may be split into two stages, beginning from a dense random packed aggregate of the powder. During stage I compaction individual contacts grow at the isolated contact points between particles. With increased macroscopic pressure each contact grows in area and strain hardens. Additionally, the number of contacts per particle increases as neighbouring particles approach and touch each other. In this paper, we examine stage I compaction, and make the simplifying assumptions that the particles are of spherical shape and of uniform size throughout the compaction process. When the relative density D has reached about 0.9, the contacts have grown sufficiently for them to touch each other. From a modelling point of view, it is then best to consider the material as a solid containing a non-dilute distribution of voids. This is stage II compaction.

Ashby and co-workers (see for example Helle *et al.*, 1985) have developed simple

expressions for both stage I and stage II compaction under hydrostatic pressure. They consider the three deformation mechanisms of low temperature plasticity, power law creep and diffusional flow. Here we summarise their main results for stage I cold compaction. Based on Artz (1982) they find that the number of contacts per particle Z is approximated by

$$Z = 12D \tag{1.1}$$

and the average area of each contact A_c is

$$A_c = \frac{\pi}{3}\left(\frac{D-D_0}{1-D_0}\right) R_0^2 \tag{1.2}$$

where D_0 is the initial relative density and R_0 is the initial particle radius. On taking the local indentation pressure at individual contacts to be three times the uniaxial yield strength σ_y for the solid composing the particles, Helle *et al.* (1985) thereby estimate the macroscopic yield pressure p_y for cold isostatic compaction to be

$$p_y = 3D^2 \frac{(D-D_0)}{(1-D_0)} \sigma_y. \tag{1.3}$$

The role of strain hardening is neglected.

More recently, Fleck *et al.* (1992a) have used the Bishop and Hill (1951) method to estimate the macroscopic yield surface for a random aggregate made from rigid–perfectly plastic spheres. The analysis parallels the equivalent model for stage II compaction given by Gurson (1977). Fleck *et al.* assume that plastic deformation occurs in a region adjacent to the contacts between particles. The local deformation field near a contact is taken to be plane strain, and the slip line field solution of Green (1954) is used to calculate the plastic dissipation at a contact due to normal and shear loading at each contact. The particles are perfectly bonded at the contacts: in accordance with Green's slip line solution the contacts possess a shear strength equal to the shear yield strength k of the material, and a tensile cohesive strength equal to the compressive indentation strength of $(2+\pi)k/\sqrt{3} \approx 3\sigma_y$, where k is the shear yield strength. The macroscopic yield surface $\Phi(\boldsymbol{\Sigma})$ of the random aggregate is closely approximated by the expression

$$\Phi(\boldsymbol{\Sigma}) = \left(\frac{\sqrt{5}\Sigma_m}{3p_y}\right)^2 + \left(\frac{5\Sigma_e}{18p_y} + \frac{2}{3}\right)^2 - 1 = 0 \tag{1.4}$$

where $\boldsymbol{\Sigma}$ is the average macroscopic Cauchy stress in the aggregate, $\Sigma_m \equiv \frac{1}{3}\Sigma_{kk}$ is the mean stress and $\Sigma_e \equiv \sqrt{\frac{3}{2}\Sigma'_{ij}\Sigma'_{ij}}$ is the effective stress, defined in terms of the deviatoric stress $\Sigma'_{ij} = \Sigma_{ij} - \frac{1}{3}\Sigma_{kk}$

Fleck *et al.* (1992a) also give a strain hardening law for the aggregate based on the idea that plastic deformation occurs within hemispherical regions subtended by the circular contacts for each particle. The recent indentation theory of Hill *et al.* (1989) shows that, as indentation proceeds, the plastic zone at each contact spreads into undeformed material within each particle. This implies that strain hardening is much less rapid than that suggested by Fleck *et al.* (1992a). [Further details on the inden-

tation theory of Hill *et al.* (1989) are given in Appendix A.] We note in passing that a simple correction to the relation (7.7) of Fleck *et al.* (1992a)

$$F(D) = \frac{45}{\sqrt{3}} D^2 \left(\frac{D-D_0}{1-D_0}\right)^{3/2} \tag{1.5}$$

brings the predictions into line with the analysis of Hill *et al.* (1989). Here, $F(D)$ is the volume fraction of deforming material within the aggregate in the region of the contacts between particles, as discussed in Fleck *et al.* (1992a).

2. YIELD SURFACE AND THE ROLE OF INTER-PARTICLE FRICTION AND COHESIVE STRENGTH

The method of Bishop and Hill (1951) will be used to estimate the macroscopic yield surface for a random aggregate of rigid–perfectly plastic particles, along the lines outlined previously by Fleck *et al.* (1992a). Here, we shall examine the role played by friction and cohesive strength between the particles upon the macroscopic response. First, we summarise the general method and then we apply it to the case of axisymmetric straining in order to motivate a general form for the macroscopic yield locus.

A velocity field $\mathbf{v}(\mathbf{x})$ is derived throughout the porous body from a uniform macroscopic plastic strain rate $\dot{\mathbf{E}}$. The internal plastic dissipation rate per unit macroscopic volume $\dot{W}$ is calculated from the assumed velocity field. Gurson (1977) has shown that the macroscopic stress $\boldsymbol{\Sigma}$ may be calculated in a straightforward fashion by differentiation of $\dot{W}$ with respect to $\dot{\mathbf{E}}$,

$$\Sigma_{ij} = \frac{\partial \dot{W}}{\partial \dot{E}_{ij}}. \tag{2.1}$$

This formula also holds for the case of a rigid-strain hardening plastic solid.

Consider a typical contact between neighbouring particles as shown in Fig. 1(a). The relative velocity of particle I with respect to the stationary reference particle O is taken to be

$$v_i = \dot{E}_{ij} n_j 2R_0 \tag{2.2}$$

where $\mathbf{n}(\phi, \theta)$ is the unit radial vector from the centre of particle O to the centre of particle I, expressed in terms of the spherical co-ordinates (ϕ, θ). The radial component of this velocity in the direction OI moving I away from O is $v_n(\phi, \theta)$; this component of the velocity is normal to the contact between the two particles. The remaining component of the velocity $v_t(\phi, \theta)$ is tangential to the contact. Plastic deformation occurs in the vicinity of the contact, and average normal and shear tractions $\sigma_{nn}(\phi, \theta)$ and $\sigma_{nt}(\phi, \theta)$ act across the contact area. As a result the plastic dissipation per unit area of contact is

$$\dot{W}_c(\phi, \theta) = \sigma_{nn} v_n + \sigma_{nt} v_t. \tag{2.3}$$

This plastic dissipation occurs over two particles so half of it is apportioned to each

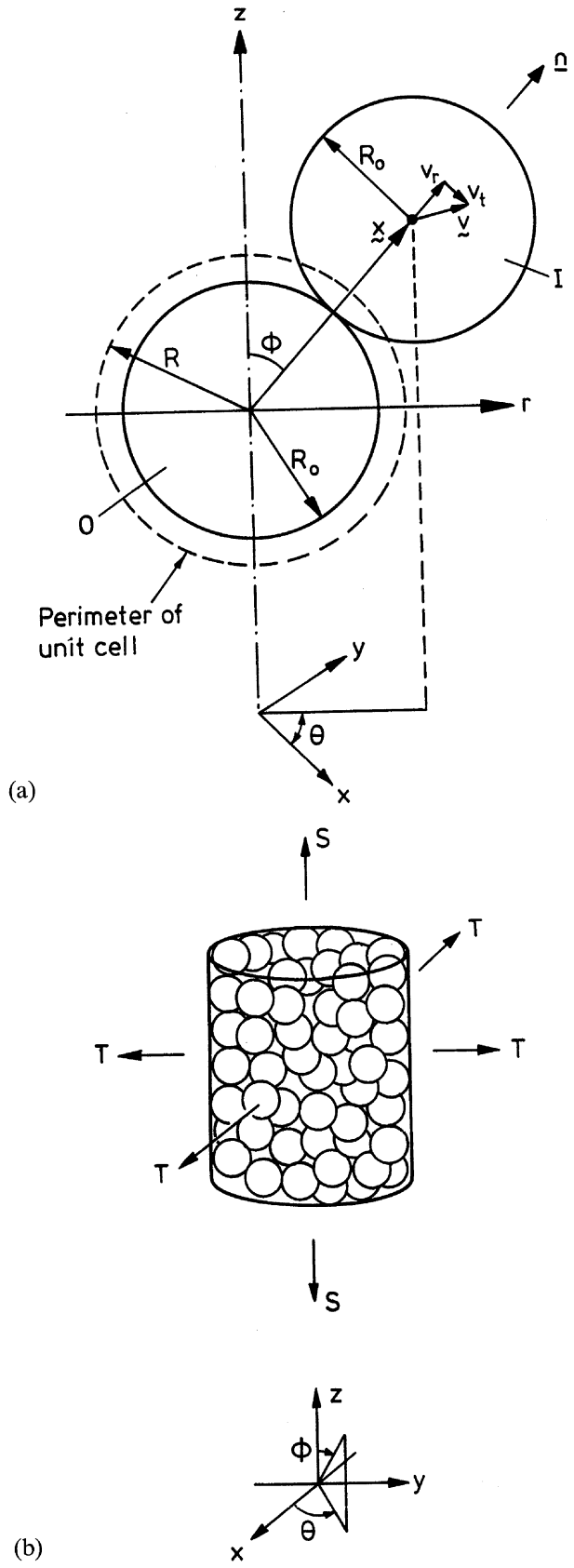

Fig. 1. (a) Typical contact between spherical particles, showing unit cell and the definition of co-ordinate systems. (b) Macroscopic element of powder aggregate under remote axisymmetric loading.

particle. Let the number of contacts per particle Z be given by (1.1) and the average contact area A_c be given by (1.2). These formulae are reasonably accurate for isostatic compaction and become progressively inaccurate with increasing component of deviatoric straining. The dissipation per particle is then given by

$$\dot{W}_p = \frac{1}{8\pi R_0^2} \int_{S_0} \{\dot{W}_c(\phi, \theta) A_c Z\} \, dS_0 \tag{2.4}$$

where integration is carried out over the particle surface S_0 of total area $4\pi R_0^2$. In order to determine the macroscopic stress $\boldsymbol{\Sigma}$ from (2.1) we calculate the dissipation per unit volume $\dot{W}$ by multiplying the plastic dissipation per particle $\dot{W}_p$ by the number of particles per unit volume, $3D/4\pi R_0^3$. Thus

$$\dot{W} = \frac{3D}{32\pi^2 R_0^5} \int_{S_0} \{\dot{W}_c(\phi, \theta) A_c Z\} \, dS_0 \tag{2.5}$$

or, upon making use of (1.1), (1.2) and (2.3)

$$\dot{W} = \frac{3D^2(D-D_0)}{8\pi R_0^3(1-D_0)} \int_{S_0} \{\sigma_{nn} v_n + \sigma_{nt} v_t\} \, dS_0. \tag{2.6}$$

2.1. *Assumed collapse mechanism*

We consider a powder aggregate made from rigid–perfectly plastic material, and restrict the local deformation field in the contacts between particles to plane strain. We may then use existing slip line field solutions to calculate $\dot{W}_p$. Following Fleck *et al.* (1992a) we start by taking the case of perfectly sticking contacts between particles. Then, the shear traction σ_{nt} at a contact is limited by the shear strength k of the material, and the maximum normal traction σ_{nn} in tension (that is, the cohesive strength) is limited by the indentation strength of $(2+\pi)k$. The slip line field solution of Green (1954) is appropriate. The nature of this slip line field depends upon the ratio v_t/v_n, which is parameterised by the angle $\alpha = \arctan(v_t/v_n)$. To simplify the discussion assume v_n is positive. [In all calculations we consider the full range of (v_n, v_t).] Then, for α in the range $-\pi/4 \leqslant \alpha \leqslant \pi/4$ the Prandtl punch field [Hill (1950)] applies and

$$\sigma_{nn} = k(2+\pi), \quad \sigma_{nt} = 0. \tag{2.7}$$

For the case $\pi/4 \leqslant \alpha \leqslant \pi/2$, the slip line field given by Green (1954) applies, and the tractions on the contact plane are

$$\sigma_{nn} = k(1+3\pi/2-2\alpha+\sin 2\alpha), \tag{2.8a}$$

$$\sigma_{nt} = -k\cos 2\alpha. \tag{2.8b}$$

Similarly, for $-\pi/2 \leqslant \alpha \leqslant -\pi/4$ Green's (1954) solution applies and

$$\sigma_{nn} = k(1+3\pi/2+2\alpha-\sin 2\alpha), \tag{2.9a}$$

$$\sigma_{nt} = k\cos 2\alpha. \tag{2.9b}$$

The solutions presented above for $v_n > 0$ apply also for $v_n < 0$ with appropriate reversals in sign in the formulae (2.7)–(2.9). Further discussion of Green's (1954) solution is given in Fleck *et al.* (1992a).

In the practical cold compaction of powders lubricants are usually added to reduce friction between the particles and between the particles and the die walls. The effect of these lubricants upon the particle–particle interaction may be gauged by considering the limit of frictionless contacts with $\sigma_{nt} = 0$. Then, the Prandtl field solution (2.7) applies for all values of α. In the following section the macroscopic yield surface is given for frictionless and fully sticking contacts, for the case of axisymmetric straining.

So far we have assumed that the dissipation at a contact for $v_n > 0$ is the same as for $v_n < 0$. Now we define the ratio of tensile cohesive strength to the normal indentation strength at a contact by the cohesion parameter η, with η in the range of zero to unity. The case $\eta = 1$ corresponds to a cohesive strength of $(2+\pi)k$ at a contact, and $\eta = 0$ corresponds to vanishing cohesive strength. We estimate the effect of a reduced cohesive strength by multiplying the expressions for $(\sigma_{nn}, \sigma_{nt})$ in (2.7)–(2.9) by the knock-down factor η in calculation of the dissipation at each contact. Explicit results are given in the following section for an axisymmetric deformation state.

2.2. *Axisymmetric deformation*

We shall estimate the macroscopic yield surface for general axisymmetric deformation, for the cases of frictionless and fully sticking particles, and η in the range of zero to unity. A general axisymmetric stress state is shown in Fig. 1(b), with the macroscopic stress components

$$\Sigma_{zz} = S, \quad \Sigma_{xx} = \Sigma_{yy} = T \tag{2.10}$$

in terms of the Cartesian reference frame (x, y, z). It is helpful to introduce two stress measures as alternatives to (S, T) in the form of a mean stress

$$\Sigma_m = \tfrac{1}{3}\Sigma_{kk} = (S+2T)/3 \tag{2.11}$$

and a measure of the deviatoric stress

$$\Sigma = S - T. \tag{2.12}$$

Note that the von Mises effective stress $\Sigma_e \equiv \sqrt{\frac{3}{2}\Sigma'_{ij}\Sigma'_{ij}}$ equals $|\Sigma|$ where $\boldsymbol{\Sigma}'$ is the macroscopic deviatoric stress tensor. The macroscopic plastic strain rate $\dot{\mathbf{E}}$ has Cartesian components $\dot{E}_{zz}$ and $\dot{E}_{xx} = \dot{E}_{yy}$, which may be re-expressed in terms of the macroscopic dilatation rate $\dot{H}$ and the distortional rate $\dot{E}$, where

$$\dot{H} = \dot{E}_{zz} + 2\dot{E}_{xx}, \quad \dot{E} = \tfrac{2}{3}(\dot{E}_{zz} - \dot{E}_{xx}). \tag{2.13}$$

The quantities $\dot{H}$ and $\dot{E}$ are the work conjugates of Σ_m and Σ, respectively: we may write the plastic dissipation rate per unit volume $\dot{W}$ as

$$\dot{W} = \Sigma_{ij}\dot{E}_{ij} = \Sigma_m \dot{H} + \Sigma\dot{E} \tag{2.14}$$

and, making use of (2.1) we calculate Σ_m and Σ by differentiation of $\dot{W}$ with respect to $\dot{H}$ and $\dot{E}$,

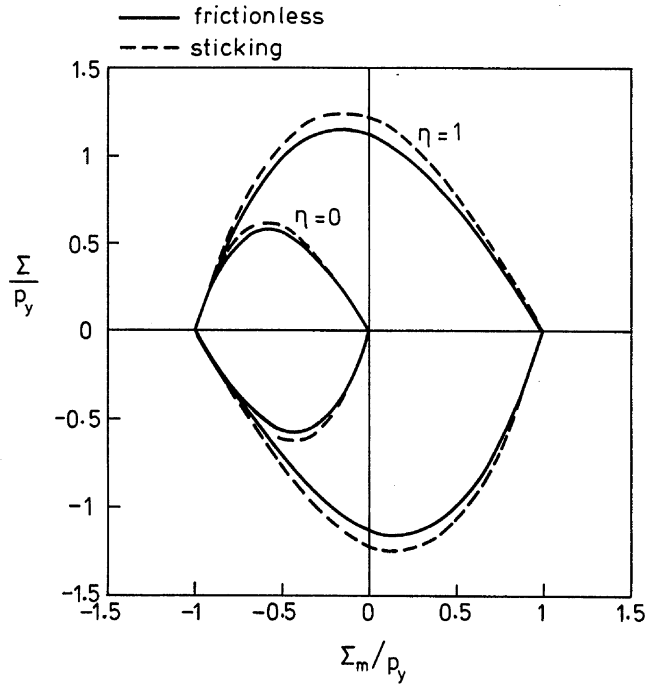

Fig. 2. Effect of inter-particle shear strength and cohesive strength upon the macroscopic yield surface, for axisymmetric loading. $\eta = 0$ corresponds to vanishing cohesive strength and $\eta = 1$ corresponds to full cohesive strength. The distribution of contacts around each particle is taken to be isotropic, and the particles are assumed to be rigid–perfectly plastic spheres.

$$\Sigma_m = \frac{\partial \dot{W}}{\partial \dot{H}}, \quad \Sigma = \frac{\partial \dot{W}}{\partial \dot{E}}. \tag{2.15}$$

In order to calculate $\dot{W}$ consider a typical contact between neighbouring particles as shown in Fig. 1(a). Given the strain rate specified in (2.13) the motion of the centre of particle I with respect to the reference particle O is, using (2.2),

$$v_n = R_0[\dot{E}(3\cos^2\phi - 1) + 2\dot{H}/3], \tag{2.16a}$$

$$v_t = -3R_0\dot{E}\sin\phi\cos\phi \tag{2.16b}$$

in terms of the spherical co-ordinate ϕ defined in Fig. 1(a). For axisymmetric deformation there is no dependence of tractions or velocities on the hoop direction, measured by the azimuth angle θ defined in Fig. 1(a). The element of surface dS_0 of the reference particle is given by $dS_0 = 2\pi R_0^2 \sin\phi\, d\phi$, and the plastic dissipation rate $\dot{W}$ follows from (2.6) as

$$\dot{W} = \frac{3D^2(D - D_0)}{4R_0} \int_0^{\pi} \{(\sigma_{nn}v_n + \sigma_{nt}v_t)\sin\phi\}\, d\phi. \tag{2.17}$$

Note that the velocities (v_n, v_t) depend upon ϕ in accordance with (2.16). The tractions $(\sigma_{nn}, \sigma_{nt})$ at the contact between the two particles are estimated from the slip line field solutions of Green (1954) and Prandtl, as described in Section 2.1.

The macroscopic yield surface is calculated by first integrating (2.17) numerically for prescribed values of $(\dot{H}, \dot{E})$. The stress state (Σ_m, Σ) corresponding to the strain rate $(\dot{H}, \dot{E})$ is then determined by differentiating numerically $\dot{W}$ with respect to $\dot{H}$ and $\dot{E}$, in accordance with (2.15). Results are given in the (Σ_m, Σ) plane in Fig. 2 for both

frictionless and fully sticking contacts, and for η in the range of zero to unity. Macroscopic stresses have been normalised in Fig. 2 with respect to the isostatic yield pressure p_y given by (1.3). The results for the fully sticking case and $\eta = 1$ have been presented previously by Fleck *et al.* (1992a). Note from Fig. 2 that the degree of friction at the contacts plays only a minor role; the yield surface for frictionless contacts lies slightly inside that for sticking contacts. This is not surprising since the value of $|\sigma_{nn}|$ in the sticking contacts is never far from the Prandtl field value of $(2+\pi)k$ and $|\sigma_{nt}| \ll |\sigma_{nn}|$ for all values of v_t/v_n. For frictionless contacts and arbitrary η, the Prandtl field is sufficiently simple for an analytical expression to be obtained for the macroscopic yield surface. For $\Sigma > 0$ we find

$$\Phi(\Sigma_m, \Sigma) = \frac{\Sigma}{p_y} - \frac{3}{2}\left(\eta - \frac{\Sigma_m}{p_y}\right)\left[1-(1+\eta)^{-2}\left(\eta - \frac{\Sigma_m}{p_y}\right)^2\right] = 0, \tag{2.18}$$

and for $\Sigma < 0$

$$\Phi(\Sigma_m, \Sigma) = \frac{\Sigma}{p_y} + \frac{3}{2}\left(1 + \frac{\Sigma_m}{p_y}\right)\left[1-(1+\eta)^{-2}\left(1 + \frac{\Sigma_m}{p_y}\right)^2\right] = 0. \tag{2.19}$$

We recognise that it is physically implausible for frictionless contacts to possess a significant cohesive strength. Since the yield surfaces for frictionless and sticking contacts are similar, we argue that relations (2.18) and (2.19) are reasonably accurate for sticking contacts over the full range $0 \leqslant \eta \leqslant 1$.

It is clear from Fig. 2 that the cohesive strength of the contacts plays a significant role for both the frictionless and sticking contacts. When $\eta = 1$ the yield surface is symmetric about the origin and the hydrostatic yield stress in tension and in compression are equal. As η is reduced in value the aggregate loses its tensile strength so that, at $\eta = 0$, the yield surface touches the origin: the tensile hydrostatic strength vanishes for $\eta = 0$.

A vertex exists where the yield surface crosses the mean stress axis Σ_m for all cases shown in Fig. 2. The right hand vertex at $\Sigma_m = \eta p_y$, $\Sigma = 0$ corresponds to tensile radial stressing with $v_n > 0$ at particle contacts of all orientations around the reference particle O in Fig. 1(a). In like manner, the vertex at $\Sigma_m = -p_y$, $\Sigma = 0$ corresponds to compressive radial stressing with $v_n < 0$ at particle contacts of all orientations.

Consider first the case of frictionless contacts and $0 \leqslant \eta \leqslant 1$. All contacts experience radial stressing of the same sign when v_n is of the same sign for all orientations ϕ. The right hand vertex at $\Sigma_m = \eta p_y$, $\Sigma = 0$ exists for $\dot{H} > 0$, and by (2.16a) $\dot{E}/\dot{H}$ lies in the range $-\frac{1}{3} \leqslant \dot{E}/\dot{H} \leqslant 2/3$. Through normality these critical values of $\dot{E}/\dot{H}$ give the angles of the yield locus at the vertex. The normal to the yield locus for $\Sigma \to 0^+$ is at an angle of $\arctan(2/3) = 33.7°$ from the horizontal Σ_m axis, and for $\Sigma \to 0^-$ is at an angle of $\arctan(-1/3) = -18.4°$ from the Σ_m axis. The vertex at $\Sigma_m = -p_y$, $\Sigma = 0$ exists for $\dot{H} < 0$, and by (2.16a) $\dot{E}/\dot{H}$ must again lie in the range $-\frac{1}{3} \leqslant \dot{E}/\dot{H} \leqslant 2/3$. The normal to the yield locus for $\Sigma \to 0^+$ (in third quadrant of stress-space) is at an angle of 18.4° from the Σ_m axis, and for $\Sigma \to 0^-$ (in fourth quadrant of stress-space) is at an angle of 33.7° from the Σ_m axis.

Now consider sticking contacts (in shear) and $0 \leqslant \eta \leqslant 1$. The two vertices for each

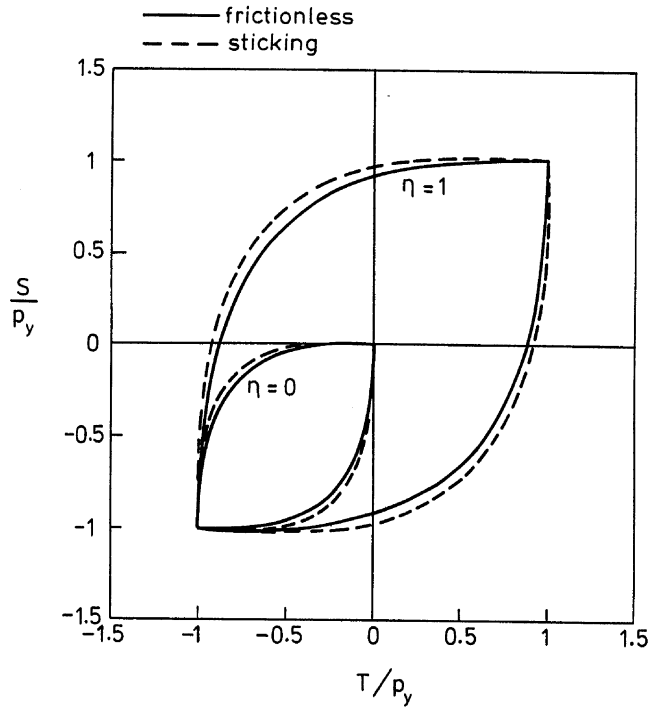

Fig. 3. Yield surface for axisymmetric loading in terms of the axial macroscopic stress S and the radial macroscopic stress T.

yield surface again correspond to radial stressing at particle contacts of all orientations. According to (2.7)–(2.9) all contacts experience radial stressing when $|\alpha| < \pi/4$, where $\alpha \equiv \arctan(v_t/v_n)$ and (v_n, v_t) are defined in (2.16). As discussed by Fleck *et al.* (1992a) the normal to the yield locus is at an angle of 22.4° from the horizontal Σ_m axis in the first and third quadrants, and at an angle of 14.3° from the Σ_m axis in the second and fourth quadrants. We note that a significant portion of the yield surface for both sticking and frictionless contacts is closely approximated by the vertices associated with the frictionless contacts, see Fig. 2.

When yielding occurs at a vertex of the macroscopic yield locus, plastic flow of the aggregate is free to follow any direction within the limiting cone of normals to the adjacent smooth segments of the yield surface. In reality, the vertex may be absent from the macroscopic yield surface for a variety of reasons. The Bishop and Hill (1951) averaging scheme is an upper bound method which gives an approximation to the actual yield surface. Strain hardening at individual contacts will also tend to round off the vertex of the macroscopic yield surface.

The existence of a vertex on the macroscopic yield surface poses a problem concerning the non-uniqueness of the direction of plastic flow. One strategy, adopted by Fleck *et al.* (1992b) is to round off the yield surface in the vicinity of the vertex. Recent experimental results on the observed yield surface for compacted copper powder by Brown and Abou-Chedid (1994) suggest that the yield surface does not possess vertices on the Σ_m axis.

The numerical results for axisymmetric deformation have been replotted in Fig. 3 using the alternative stress measures S and T. The "pure-pressure vertex" at $\Sigma_m = -p_y, \Sigma = 0$ now appears as a vertex at $S = T = -p_y$; similarly the "hydrostatic-

tension vertex" at $\Sigma_m = \eta p_y$, $\Sigma = 0$ now appears at $S = T = \eta p_y$. The yield surfaces in the (T, S) plane can be interpreted in the following approximate manner. In the first quadrant the aggregate yields when the principal stress with the larger magnitude attains a yield value of ηp_y. Similarly, in the third quadrant the aggregate yields when the principal stress with the largest absolute value attains $-p_y$. By the normal plastic flow rule, the vector with components $(2\dot{E}_{xx}, \dot{E}_{zz})$ is oriented normal to the yield surface at the position (T, S). The shapes of the yield surfaces for both frictionless and sticking contacts and $0 \leqslant \eta \leqslant 1$ are such that, in the first and third quadrants, plastic flow is almost aligned with the direction of the larger principal stress. At the vertices $S = T$ (in the first and third quadrants of $S-T$ space), plastic flow can range from nearly uniaxial straining through purely hydrostatic straining to almost plane strain. In the second and fourth quadrants of (T, S) space yielding occurs with some combination of axial and transverse straining.

2.3. *Comparison with the Cam Clay model*

The yield surface for $\eta = 0$ bears some resemblance to the empirical Cam Clay soil mechanics model developed by Schofield and Wroth (1968). In the absence of elasticity the Cam Clay yield surface is

$$\Phi(\Sigma_m, \Sigma) = \left(\frac{\Sigma_m}{p_y} + 1\right)^2 + \left(\frac{\Sigma}{M p_y}\right)^2 - 1 = 0 \tag{2.20}$$

where p_y is the hydrostatic yield pressure, and M is a constant of order unity. Schofield and Wroth found experimentally that the hydrostatic yield pressure varies with relative density D according to

$$p_y = p_0 \exp\left(-\frac{1}{\lambda D}\right) \tag{2.21}$$

where the constants p_0 and λ are measured by curve fitting (2.21) to experimental data. Clearly, the densification relation (2.21) is of a different functional form to that given by (1.3). (By judicious choice of p_0 and λ the two relations may be brought into approximate coincidence over a small range of D.)

The Cam Clay yield surface (with $M = 1$) is compared in Fig. 4 with the yield surface generated in the current study for frictionless contacts. Qualitatively, the two yield surfaces are of similar form; the most striking difference is the absence of vertices on the Cam Clay yield surface. Nonetheless, the degree of similarity leads us to conclude that the contact yielding model provides a possible micromechanical basis for the empirical Cam Clay model.

3. ANISOTROPIC CONSTITUTIVE LAW

So far we have assumed that the contacts between particles are of uniform area and are distributed around each particle in an isotropic manner. Further, the degree of strain hardening is taken to be the same at each contact. An anisotropic yield law

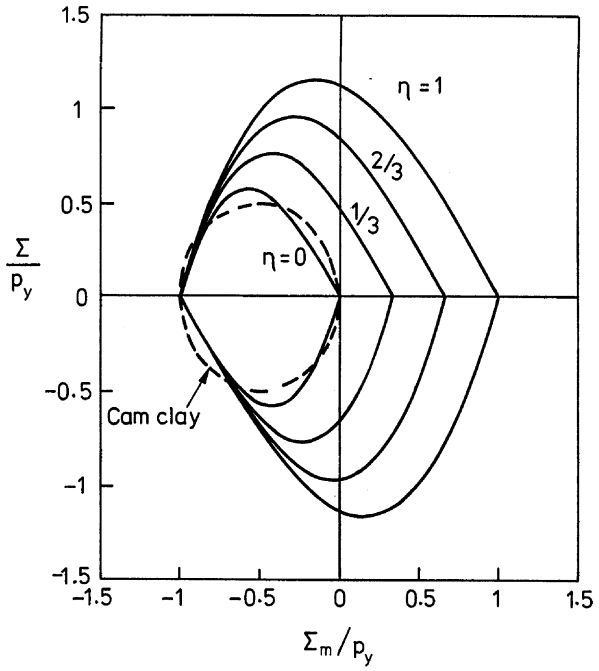

Fig. 4. Comparison of yield surface for an isotropic distribution of contacts with the empirical Cam Clay model used in soil mechanics.

may be developed for stage I compaction by assuming that an appropriate second order tensor **B** describes (i) the distribution of contact area, (ii) the number of contacts per unit surface area of particle and (iii) the hardness of each contact. For the case of hydrostatic loading **B** reduces to the relative density D.

The anisotropic constitutive law is developed from the above isotropic theory, so that it reduces to the isotropic result in the case of hydrostatic loading. We have already noted that inter-particle friction plays only a secondary role in influencing the yield surface, and so we make the simplifying assumption of frictionless contact between particles. The yield surface for the rigid-strain hardening solid is derived from (2.1), where the plastic dissipation rate per unit current volume $\dot{W}$ is given by a slightly modified form of (2.5),

$$\dot{W} = \frac{3D}{8\pi R_0^3} \int_{S_0} \{\dot{W}_c(\phi, \theta) A_c z\} \, dS_0. \tag{3.1}$$

Here, the area of a contact A_c and the number of contacts z per unit area of particle are taken to vary spatially over the surface of the particle in a manner which will be made precise below. The plastic dissipation per unit area of contact $\dot{W}_c$ is given by

$$\begin{aligned} \dot{W}_c &= -\bar{p} v_n, \quad v_n < 0, \\ \dot{W}_c &= \eta \bar{p} v_n, \quad v_n \geqslant 0 \end{aligned} \tag{3.2}$$

where v_n is the normal contact velocity of one particle relative to a reference particle and $\bar{p}$ is the contact pressure at a contact. (For the case of vanishing strain hardening $\bar{p} = 3\sigma_y$.) On denoting the unit vector along the line of centres of two particles by **n**, as shown in Fig. 1(a), the normal contact velocity v_n is

$$v_n = n_i v_i = \dot{E}_{ij} n_i n_j 2R_0 \tag{3.3}$$

where the relative velocity $\mathbf{v}$ has already been defined by (2.2).

The contact size of a contact A_c, the number of contacts per unit area z and the local indentation pressure $\bar{p}$ at a contact are all taken to vary over the surface of the representative particle. Consider first the contact size of a contact A_c. We assume that A_c varies over the surface of the particle according to

$$A_c = 4\pi R_0^2 n_i n_j B_{ij} \tag{3.4}$$

where $\mathbf{B}$ is deduced from indentation theory. To proceed, we determine the functional dependence of the Jaumann rate $\overset{*}{\mathbf{B}}$ of $\mathbf{B}$ upon $\dot{\mathbf{E}}$. Consider two spherical particles of radius R_0 made from a J_2 deformation theory solid (of uniaxial response $\varepsilon = (\sigma/\sigma_0)^n$ where n is the strain hardening exponent in the range of unity to infinity, and σ_0 is a material constant). When two spherical particles of radii R_0 are pressed together by a total inter-penetration of $2h$, the area of contact A is given by

$$A = 2\pi c^2 h R_0. \tag{3.5}$$

Hill *et al.* (1989) show that the constant c^2 varies from $c^2 = 0.5$ for $n = 1$ to $c^2 \approx 4/3$ for $n = \infty$. Now imagine that the two particles form part of the powder aggregate; the normal contact velocity v_n between the spheres is

$$v_n = -2\dot{h} \tag{3.6}$$

and the rate of growth of the area of contact between the spheres follows from differentiation of (2.6) with respect to time, as

$$\dot{A} = -\pi c^2 R_0 v_n. \tag{3.7}$$

We conclude via (3.3) and (3.6) that $\dot{A}$ scales with the macroscopic strain rate $\dot{\mathbf{E}}$ according to

$$\dot{A} \propto R_0^2 n_i n_j \dot{E}_{ij}. \tag{3.8}$$

An expression for the Jaumann rate $\overset{*}{\mathbf{B}}$ is obtained by differentiating (3.4) with respect to time, and by equating the resulting expression for $\dot{A}_c$ with that for $\dot{A}$; hence,

$$\overset{*}{B}_{ij} \propto \dot{E}_{ij}. \tag{3.9}$$

The "constant of proportionality" between $\overset{*}{\mathbf{B}}$ and $\dot{\mathbf{E}}$ in (3.8) is obtained by calibrating (3.4) to reduce to the formula (1.2) in the hydrostatic limit. The rate form of (1.2) gives

$$\dot{A}_c = -\frac{\pi}{3} \frac{D}{(1-D_0)} R_0^2 \dot{E}_{kk}. \tag{3.10}$$

Under purely hydrostatic straining, (3.4) gives

$$\dot{A}_c = 4\pi R_0^2 n_i n_j \overset{*}{B}_{ij} \tag{3.11}$$

and, upon comparing the above two expressions, we deduce that $\overset{*}{\mathbf{B}}$ is related to $\dot{\mathbf{E}}$ by

$$\overset{*}{B}_{ij} = -\frac{1}{4}\frac{D}{(1-D_0)}\dot{E}_{ij}. \tag{3.12}$$

The above formula for $\overset{*}{\mathbf{B}}$ is used to update the internal state variable $\mathbf{B}$.

Now consider the local hardness $\bar{p}$ at each individual contact. The average indentation pressure $\bar{p}$ for mutual indentation of two power-law hardening plastic spheres is given by Johnson (1985) and Hill *et al.* (1989)

$$\bar{p} = 3\sigma_0\left(\frac{0.04A_c}{\pi R_0^2}\right)^{1/2n} \tag{3.13}$$

where n is the strain hardening exponent. Hence, the local hardness at each contact varies with position over a representative particle as stipulated by (3.13) and (3.4).

To complete the specification for $\dot{W}$ in (3.1) we must determine how the number of contacts per unit area of particle surface z depends upon the tensor $\mathbf{B}$. We assume that $\dot{z}(\mathbf{n})$ is linear in the normal velocity v_n between two particles, so that

$$\dot{z} \propto n_i n_j \dot{E}_{ij}. \tag{3.14}$$

In the hydrostatic limit $z = Z/4\pi R_0^2$ is given by (1.1), and

$$\dot{z} = -\frac{3D}{\pi R_0^2}\dot{E}_{kk}. \tag{3.15}$$

Comparison of (3.14) and (3.15) provides the constant of proportionality in (3.14) as $-9D/\pi R_0^2$ for arbitrary straining. The rate $\dot{z}$ may be phrased in terms of $\overset{*}{\mathbf{B}}$ instead of $\dot{\mathbf{E}}$ by making use of (3.12) to give,

$$\dot{z} = \frac{36(1-D_0)}{\pi R_0^2} n_i n_j \overset{*}{B}_{ij}, \tag{3.16}$$

which may be integrated directly to give,

$$z = \frac{36(1-D_0)}{\pi R_0^2} n_i n_j B_{ij} + \frac{3D_0}{\pi R_0^2}. \tag{3.17}$$

In summary, $\mathbf{B}$ defines the material state during compaction. For a given value of $\mathbf{B}$, the macroscopic stress $\boldsymbol{\Sigma}$ is calculated from (2.1), with $\dot{W}$ given by (3.1). Since $\dot{W}$ is homogeneous of degree one in $\dot{\mathbf{E}}$, the value of $\boldsymbol{\Sigma}$ depends upon the assumed direction of $\dot{\mathbf{E}}$. The current yield surface is mapped out by selecting all possible directions of $\dot{\mathbf{E}}$. Some examples of the evolution of yield surface given by the above model are given in the following section for axisymmetric loading. In a more general implementation of the scheme it is best to differentiate (2.1) analytically, and integrate (3.1) numerically over the surface of the reference particle.

The tangent modulus $\mathbf{L}$ relates the Jaumann stress increment $\overset{*}{\boldsymbol{\Sigma}}$ to the strain rate $\dot{\mathbf{E}}$ by

$$\overset{*}{\Sigma}_{ij} = L_{ijkl}\dot{E}_{kl}. \tag{3.18}$$

In general, $\mathbf{L}$ is homogeneous and of degree zero in $\dot{\mathbf{E}}$. When loading is proportional or nearly so, continued loading of active contacts occurs and $\mathbf{L}$ is obtained by

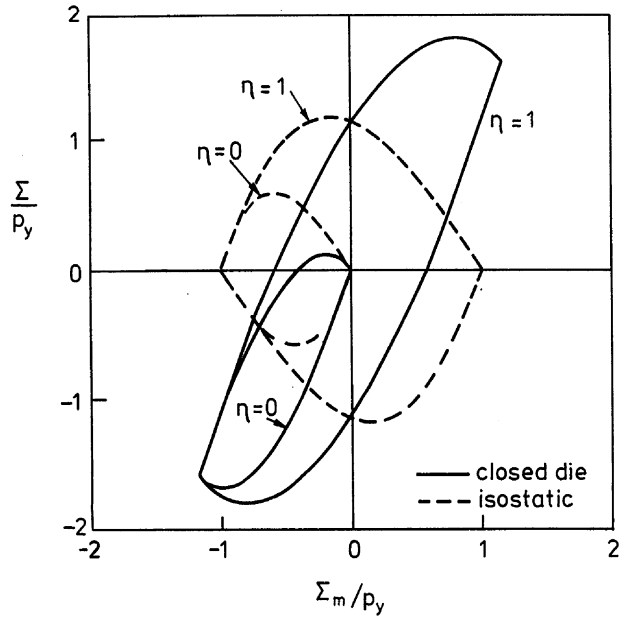

Fig. 5. Effect of strain path on the evolution of yield surface, according to the anisotropic theory. The yield surface is given for both isostatic compaction (hydrostatic strain history) and closed die compaction (uniaxial strain state with $E_{xx} = E_{yy} = 0$). Contacts are frictionless between particles, and the two limits of full cohesive strength $\eta = 1$ and zero cohesive strength $\eta = 0$ are presented. The powder has been compacted to a relative density $D = 0.8$ from an initial density $D_0 = 0.64$.

differentiation of (2.1) with respect to time. In the more general loading case, unloading of some of the contacts occurs and it is difficult to extract an explicit expression for **L**.

4. PREDICTIONS OF THE ANISOTROPIC CONSTITUTIVE LAW FOR AXISYMMETRIC LOADING

Consider the powder aggregate in an initial isotropic state and subjected to the axisymmetric stress state shown in Fig. 2. The anisotropic constitutive law simplifies considerably for the case of proportional axisymmetric straining, where $\dot{E} = \lambda \dot{H}$. Then, $\dot{\mathbf{B}}$ may be integrated to give

$$B_{ij}n_in_j = \frac{1}{12}\left(\frac{D-D_0}{1-D_0}\right)[(1-\tfrac{3}{2}\lambda)\sin^2\phi + (1+3\lambda)\cos^2\phi] \tag{4.1}$$

in terms of the spherical co-ordinate ϕ defined in Fig. 1.

The predicted shape of the macroscopic yield surface is shown in Fig. 5 for both isostatic compaction ($E = 0$) and closed die compaction ($E_{xx} = E_{yy} = 0$). We take the case of ideally plastic behaviour $n = \infty$, and show the effect of inter-particle cohesion by taking the two limits of $\eta = 0$ and $\eta = 1$ in the expression (3.2) for $\dot{W}_c$. It is clear from Fig. 5 that the strain path has a major influence on the shape of the yield surface. In all cases a corner exists at the loading point of the yield surface. This is similar to the development of a corner at the loading point in crystal plasticity theory for

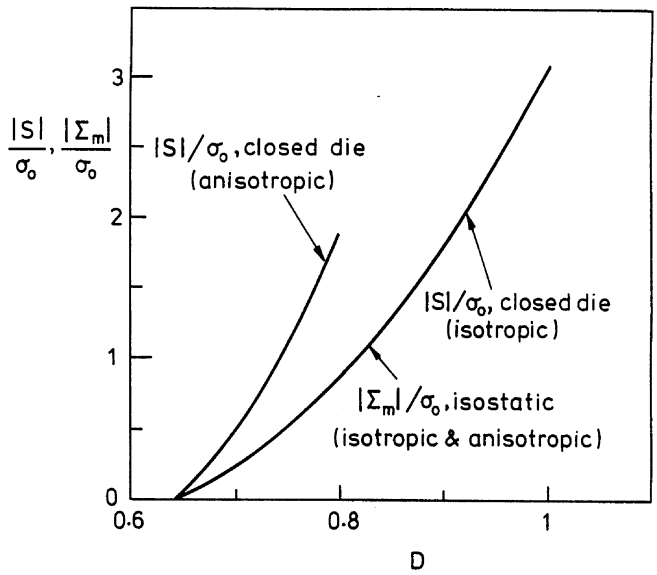

Fig. 6. Macroscopic stress versus strain response for isostatic compaction and closed die compaction. The anisotropic theory is calibrated against the isotropic theory to give the same response under isostatic straining. For closed die compaction, the anisotropic theory predicts a stiffer response than the isotropic theory.

independent hardening or mild latent hardening (where the cross-hardening from one slip system to the next is less than the self-hardening on the active slip systems). The yield surface for isostatic compaction is the same as that given previously in Fig. 2 for the isotropic model: this is fully expected as the anisotropic model is calibrated against the isotropic model for the case of isostatic loading.

Macroscopic stress–strain responses are given in Fig. 6 for both the anisotropic theory and the isotropic hardening theory of Fleck *et al.* (1992a). We consider the ideally plastic limit $n = \infty$ and assume the initial relative density $D_0 = 0.64$. The strain measure used is the relative density D: for the case of isostatic compaction D is related to the true hydrostatic strain H by $D = D_0 \exp(-H)$, and for closed die compaction D is related to the only non-vanishing strain component E_{zz} by $D = D_0 \exp(-E_{zz})$. (Note that $H = E_{zz}$ for closed die compaction). Since the anisotropic theory has been calibrated against the isotropic theory in the limit of isostatic straining the isotropic hardening and anisotropic hardening theories give identical predictions for isostatic compaction.

For closed die compaction the anisotropic theory predicts substantially greater hardening along the direction of straining than the isotropic theory of Fleck *et al.* (1992a). This is due to the fact that the anisotropic theory gives both larger contacts and a larger number of contacts along the direction of straining (z axis) than the isotropic theory. The isotropic hardening theory predicts a purely hydrostatic stress state for a strain state of closed die compaction, as a consequence of the vertex on the hydrostatic stress axis of the yield surface shown in Fig. 5. In fact, the isotropic theory predicts an identical stress state at a given value of D for closed die compaction and for isostatic compaction, see Fig. 6. It is thought that the anisotropic theory is more physically realistic than the isotropic hardening theory since it attempts to model geometric hardening due to growth of the contacts between particles along the direction of macroscopic straining.

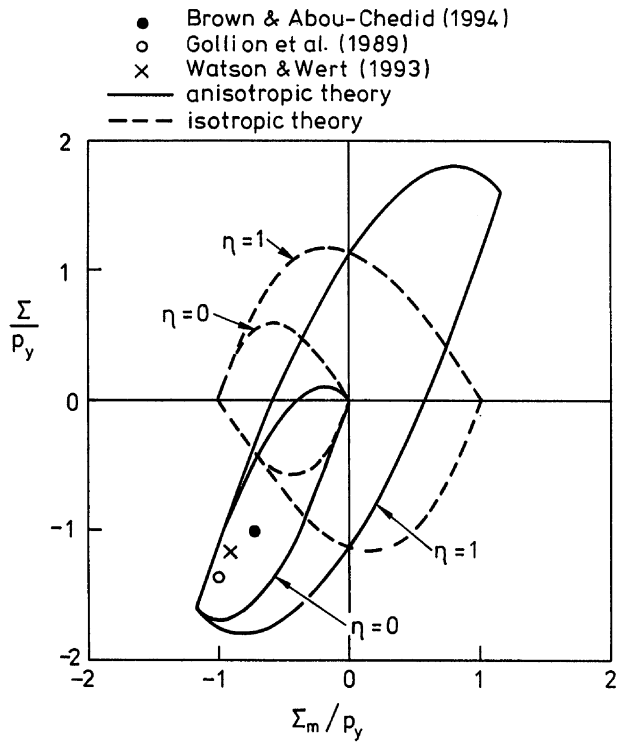

Fig. 7. Comparison of yield surface with experimental data for closed die compaction. The experimental data are for gas atomised copper powder (Brown and Abou-Chedid, 1994), iron powder (Gollion *et al.*, 1989) and for aluminium powder (Watson and Wert, 1993).

4.1. *Comparison with experimental observations*

A number of investigators have examined experimentally the compaction response of metal powders for both closed die compaction and isostatic compaction (Koerner and Quirus, 1971; Gollion *et al.*, 1989; Watson and Wert, 1993; Brown and Abou-Chedid, 1994). We shall now argue that the anisotropic constitutive law has some success in predicting the closed die compaction response.

Measured values of deviatoric stress $\Sigma \equiv S-T$ and mean stress $\Sigma_m \equiv \frac{1}{3}S+\frac{2}{3}T$ are plotted in Fig. 7, for closed die compaction from an initial relative density of $D_0 \approx 0.64$. In each case, the data refer to a relative density D of 0.8, and values for p_y have been chosen to equal the measured pressure in an isostatic compaction to $D = 0.8$. The predictions of both the isotropic theory and the anisotropic theory are included in the figure. The experimental data clearly show that the stress state in closed die compaction is not isostatic; both the data and the anisotropic model suggest that $\Sigma/\Sigma_m \approx 1.4$ whereas the isotropic theory gives $\Sigma = 0$. The magnitude of stresses given by the anisotropic theory for closed die compaction is in reasonable agreement with the measured stress state; there is some indication that the anisotropic theory is stronger than the experimentally observed response.

Next we compare the magnitude of axial stress Σ_{zz} in closed die compaction with the magnitude of hydrostatic stress Σ_m in isostatic compaction, in order to compact a powder to the same relative density D, from an initial density $D_0 = 0.64$. For the ideally plastic solid, the anisotropic theory predicts $\Sigma_m/\Sigma_{zz} = 0.50$ and the isotropic theory gives $\Sigma_m/\Sigma_{zz} = 1$, independent of the degree of compaction. Experimental

data for cold compaction of metal powders suggest that Σ_m/Σ_{zz} lies in the range $\Sigma_m/\Sigma_{zz} = 0.45$–$0.78$, and is almost independent of D for stage I compaction $D < 0.9$ (Koerner and Quirus, 1971; Gollion *et al.*, 1989; Watson and Wert, 1993; Brown and Abou-Chedid, 1994).

We conclude that the anisotropic theory is in broad agreement with the experimental observations for closed die compaction.

5. CONCLUDING REMARKS

In this paper the roles of inter-particle friction, cohesive strength and anisotropy have been examined for stage I cold compaction of spherical powders. It is assumed that the compaction mechanism is rate independent plasticity at the contacts between particles. We find that the magnitude and shape of the macroscopic yield locus are strongly influenced by the magnitude of the cohesive strength between particles and by the non-uniform development of contacts around each particle; in contrast, the level of inter-particle friction has only a minor influence on the bulk behaviour. Both the isotropic and the anisotropic constitutive laws are based on the kinematic assumption (2.2) that the relative velocity between two neighbouring particles follows directly from the macroscopic strain rate. This assumption is reasonable for straining which is close to hydrostatic, but becomes less accurate when the strain rate involves a significant deviatoric component. An alternative scheme is to assume that the macroscopic strain rate is the sum of the strain rate contributions from all contacts surrounding a particle; only those contacts which are instantaneously yielding contribute to the macroscopic strain rate. In this manner a theory may be developed along the lines of crystal plasticity theory. Such a theory would show in a more accurate fashion the role of inter-particle shear strength upon the macroscopic yield surface. Some initial steps in the development of such a theory have already been taken by Calladine (1971), and the approach would merit further study.

ACKNOWLEDGEMENTS

The financial support of ARPA is gratefully acknowledged (collaborative program with the University of Virginia under the contract number 0014-91-J-4089). The author wishes to thank Dr A. C. F. Cocks and Professor M. F. Ashby for helpful discussions.

REFERENCES

Artz, E. (1982) The influence of an increasing particle co-ordination on the densification of spherical powders. *Acta Metall.* **30,** 1883–1890.

Bishop, J. F. D. and Hill, R. (1951) *Phil. Mag.* **42,** 1298.

Brown, S. B. and Abou-Chedid, G. (1994) *J. Mech. Phys. Solids* **42**(3), 383.

Calladine, C. R. (1971) A microstructural view of the mechanical properties of saturated clay. *Geotechnique* **21,** 319–415.

Fischmeister, H. F., Artz, E. and Olsson, L. R. (1978) Particle deformation and sliding during

compaction of spherical powders: a study by quantitative metallography. *Powder Metall.* **21**(4), 179–187.
Fleck, N. A., Kuhn, L. T. and McMeeking, R. M. (1992a) Yielding of metal powder bonded by isolated contacts. *J. Mech. Phys. Solids* **40**(5), 1139–1162.
Fleck, N. A., Otoyo, H. and Needleman, A. (1992b) Indentation of porous solids. *Int. J. Solids Struct.* **29**(13), 1613–1636.
Gollion, J., Bouvard, D., Stutz, P., Grazzini, H., Levaillant, C., Baudin, P. and Cescutti J. P. (1989) On the rheology of metal powder during cold compaction. *Proc. Int. Conf. on Powders and Grains* (ed. Biarez and Gourves), pp. 433–438, 4–8 September 1989, Clermont-Ferrand, France.
Green, A. P. (1954) The plastic yielding of metal junctions due to combined shear and pressure. *J. Mech. Phys. Solids* **2,** 197–211.
Gurson, A. L. (1977) *Trans. ASME Ser. H, J. Engng Mater. Technol.* **99,** 2.
Helle, A. S., Easterling, K. E. and Ashby, M. F. (1985) Hot-isostatic pressing diagrams: new developments. *Acta Metall.* **33**(12), 2163–2174.
Hill, R. (1950). *The Mathematical Theory of Plasticity*. Oxford University Press.
Hill, R., Storakers, B. and Zdunek, A. B. (1989) A theoretical study of the Brinell hardness test. *Proc. Roy. Soc. Lond.* **A436,** 301–330.
Johnson, K. L. (1985) *Contact Mechanics*. Cambridge University Press.
Kaker, A. K. and Chaklader, A. C. D. (1967) *J. Appl. Phys.* **38,** 3223.
Koerner R. M. and Quirus F. J. (1971) High density P/M compacts utilizing shear stresses. *Int. J. Powder Metall.* **7**(3), 3–9.
Mason, G. (1968) *Nature* **217,** 733.
Schofield, A. and Wroth, C. P. (1968) *Critical State Soil Mechanics*. McGraw Hill.
Scott, G. D. (1962) *Nature* **194,** 956.
Watson, T. J. and Wert, J. A. (1993) On the development of constitutive relations for metallic powders. *Metall. Trans. A* **24A,** 2071–2081.

APPENDIX A: ESTIMATION OF YIELD SURFACE FOR DENSE RANDOM PACKING

In this appendix, we calculate the distribution of number and size of contacts around a representative particle in a powder aggregate. The powder is taken to be initially in a state of dense random packing, and is subjected to proportional axisymmetric straining. Once the distribution of contact size is known, the macroscopic yield surface is estimated via a relation of the form (2.1).

Size and number of contacts for axisymmetric compaction

The total area of contacts per particle depends upon the strain state as follows. We assume that spherical powder of uniform radius R_0 exists in a state of dense random packing prior to compaction. A representative spherical particle of radius R_0 is placed at the chosen origin of a spherical co-ordinate system as shown in Fig. 1(a). When the aggregate is subjected to a uniform state of true strain $\mathbf{E}$ it is assumed that a neighbouring particle with centre located initially at $\mathbf{r}$ moves to a location $\mathbf{R} = \mathbf{F} \cdot \mathbf{r}$, in terms of the deformation gradient $\mathbf{F} = e^{\mathbf{E}}$. Provided $\mathbf{R} \equiv |\mathbf{R}| < 2R_0$ the two particles are in contact with a finite area of contact A. We estimate A by employing the indentation theory outlined by Hill *et al.* (1989). They consider normal indentation of a half-space made from a power-law hardening plastic solid by a rigid ball of radius R_0. The uniaxial tensile response of the plastic solid is taken as $\varepsilon = (\sigma/\sigma_0)^n$ where n is the strain hardening exponent in the range of unity to infinity, and σ_0 is a material constant. Hill *et al.* find that the contact area A varies with the penetration h of the indenter according to

$$A = 2\pi c^2 h R_0. \tag{A.1}$$

The constant c^2 is a function only of n and varies from a value of 0.5 for $n = 1$ to a value of approximately 4/3 for $n = \infty$. In the present context the penetration h is defined by $h = 2R_0 - R$, for $R < 2R_0$. Relation (A.1) is the same as (3.5) and has been repeated here for the sake of convenience.

In order to calculate the total area of contact for the representative particle placed at the origin, we need to specify the distribution of neighbouring particles in a dense random packing. Let the cumulative radial density function $G(r)$ denote the cumulative number of neighbouring particle centres within a fictitious sphere of radius r around a central reference sphere. Scott (1962) and Mason (1968) have determined $G(r)$ for dense random packing. Their results show that $G(r)$ can be adequately approximated by Artz (1982),

$$G(r) = Z_0 + C\left(\frac{r}{2R_0} - 1\right), \quad r \geqslant 2R_0 \tag{A.2}$$

where $Z_0 = 7.3$ and $C = 15.5$. The radial density function $g(r)$ is given by

$$g(r) \equiv \frac{dG}{dr} = 2(Z_0 - 2C)\delta(r - 2R_0) + \frac{C}{2R_0}, \quad r \geqslant 2R_0 \tag{A.3}$$

where δ is the Dirac delta function. Relation (A.3) is the probability density function for particle contacts, for particles with an initial centre–centre spacing of r.

To proceed, consider the case of a dense random packing subjected to the axisymmetric strain field $(E_{xx}, E_{yy} = E_{xx}, E_{zz})$. Since deformation is axisymmetric and the arrangement of particles is isotropic the location of the centre of a representative particle may be represented by the spherical polar co-ordinates (r_0, ϕ_0) in the undeformed state and by (R, ϕ) in the deformed state. (Without loss of generality the azimuth angle $\theta = 0$.) We assume that the central reference particle is in contact with a neighbouring particle if $R < 2R_0$.

The total area of contact around a representative particle in the deformed configuration A_t due to contact with neighbouring particles initially in a dense random configuration follows from (A.1) and (A.3) as

$$A_t = \int_0^{\pi/2} d\phi_0 \int_{2R_0}^{r_l} dr\{Ag(r)\} \tag{A.4a}$$

$$= \int_0^{\pi/2} d\phi_0 \int_{2R_0}^{r_l} dr\left\{\pi c^2 R_0(2R_0 - R)\left[Z_0\delta(r_0 - 2R_0) + \frac{C}{2R_0}\right]\right\} \tag{A.4b}$$

where $r = r_l$ corresponds to $R = 2R_0$ in the deformed state. A straightforward kinematic relation exists between r and R of the form $r = \beta R$ where the geometrical factor β is given by

$$\beta = (e^{-2E_{xx}} \sin^2\phi + e^{-2E_{zz}} \cos^2\phi)^{1/2} \tag{A.5a}$$

in terms of the axisymmetric strain state $(E_{xx}, E_{yy} = E_{xx}, E_{zz})$, and by

$$\beta = e^{-H/3}(e^{E} \sin^2\phi + e^{-2E} \cos^2\phi)^{1/2} \tag{A.5b}$$

in terms of the reduced strain variables $E = \frac{2}{3}(E_{zz} - E_{xx})$ and $H = E_{zz} + 2E_{xx}$. Thus $r_l = \beta 2R_0$ and (A.4b) may be integrated over r to give

$$A_t = \pi c^2 R_0^2 \int_0^{\pi/2} \left\{\sin\phi_0\left[2Z_0\left(\frac{\beta - 1}{\beta}\right) + C\left(\beta + \frac{1}{\beta} - 2\right)\right]\right\} d\phi_0. \tag{A.6}$$

The total area of contact A_t may be written in terms of the spherical co-ordinate ϕ in the deformed configuration as

$$A_t = \int_{S_0} \rho(N)\, \mathrm{d}S_0 = 4\pi R_0^2 \int_0^{\pi/2} \rho(\mathbf{N}) \sin\phi\, \mathrm{d}\phi \tag{A.7}$$

where $\mathbf{N}$ is the unit outward normal to the surface S_0 of the representative particle in the deformed configuration and $\rho(\mathbf{N})$ is the probability density function of contact area over the representative particle. Comparison of (A.6) and (A.7) provides an expression for $\rho(\mathbf{N})$ as

$$\rho(\mathbf{N}) = \frac{c^2}{4} \frac{\mathrm{e}^{-H}}{\beta^3} \left[2Z_0 \left(\frac{\beta - 1}{\beta} \right) + C\left(\beta + \frac{1}{\beta} - 2 \right) \right]. \tag{A.8}$$

An expression may also be obtained for the total number of contacts Z due to axisymmetric compaction of a dense random array of particles. The approach is essentially the same as for calculation of contact size; the reference particle is in contact with a neighbouring particle if, in the deformed configuration, $R < 2R_0$. The resulting expression for Z is

$$Z = \int_0^{\pi/2} \left\{ \sin\phi \frac{\mathrm{e}^{-H/3}}{\beta^3} (Z_0 + C(\beta - 1)) \right\} \mathrm{d}\phi. \tag{A.9}$$

Calculation of macroscopic yield locus for axisymmetric compaction

The macroscopic yield surface may be calculated from the assumed distribution (A.7) of contact size over the reference particle. Consider the case of frictionless particles with ideal cohesive strength $\eta = 1$. With the relative normal velocity v_n between particles given by (2.16a), and the local contact pressure at a contact given by (2.7), the plastic dissipation rate per unit volume $\dot{W}$ follows from (2.4) and (A.7) as

$$\dot{W} = \frac{1}{2} \frac{3D}{4\pi R_0^3} \int_{S_0} \{\sigma_{nn} |v_n| \rho(\mathbf{N})\}\, \mathrm{d}S_0. \tag{A.10}$$

The macroscopic yield locus for a given state of prior strain is determined by numerical differentiation of $\dot{W}$ with respect to $\dot{\mathbf{E}}$ as stipulated by (2.1).

A comparison is given in Fig. A1 of the macroscopic yield surface predicted from an assumed dense random packing arrangement and the yield surface derived from the anisotropic constitutive law (described in Section 3 of the main text). We neglect strain hardening at the material level, and show the yield surfaces for both isostatic compaction and closed die compaction, at a relative density $D = 0.7$ from an assumed initial density of $D_0 = 0.64$. The magnitude of the yield surface in the dense random packing model is somewhat sensitive to the assumed value of the constant c^2. We take $c^2 = 4/3$ which is appropriate for $n = \infty$ in the Hill *et al.* (1989) indentation theory (see A.1). In general Fig. A1 shows excellent agreement between the predictions of the anisotropic model and the dense random packing model. This provides further theoretical support to the accuracy of the anisotropic theory.

Size and number of contacts for isostatic compaction

Helle *et al.* (1985) have given simple analytical formulae for the number of contacts per particle (equation (1.1) of the current paper) and for the average area of each contact A_c (1.2), for the case of isostatic compaction. Their estimates are based on the idealised calculations of Artz (1982). Here, we present a more rigorous calculation for the case of stage I compaction, and show that the simple relations given by Helle *et al.* (1985) are adequate for practical purposes.

The number of contacts per particle depends upon hydrostatic strain by a simplified version of the above argument for axisymmetric straining. During compaction, the relative density D increases from the dense random packing value $D_0 = 0.64$, and the centre–centre spacing between two representative particles is reduced from r to

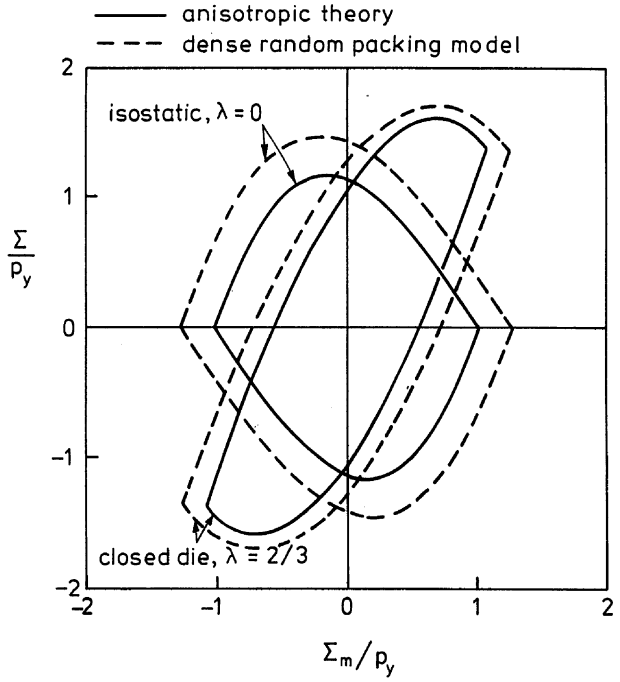

Fig. A1. Comparison of yield surface given by anisotropic theory and the dense random packing model, for isostatic compaction and closed die compaction. Initial density $D_0 = 0.64$ and current density $D = 0.8$. Stresses have been normalised by the isostatic yield strength p_y given by (1.3).

$$R = r\left(\frac{D_0}{D}\right)^{1/3}. \tag{A.11}$$

We assume that contact occurs between two particles if R is less than $2R_0$. Then, the total number of contacts per particle Z as a function of D is given by

$$Z = \int_{2R_0}^{2R_0(D/D_0)^{1/3}} \{g(r)\}\, \mathrm{d}r, \tag{A.12}$$

which reduces to

$$Z = Z_0 + C\left[\left(\frac{D}{D_0}\right)^{1/3} - 1\right] \tag{A.13}$$

via (A.3). The prediction (A.13) appears to be slightly more accurate than the formula (1.1) of Helle *et al.* (1985), when compared against the experimental data of Fischmeister *et al.* (1978), see Fig. A2.

Now consider the total area of contact per particle. Consider two representative particles in a dense random packed aggregate; the particles have an initial centre–centre spacing of $r \geqslant 2R_0$. When the relative density is increased from the initial value D_0 to the current value D, the spacing decreases to a value R given by (A.11). The overlap between the two particles is $2h = 2R_0 - R$ provided $R \leqslant 2R_0$, and the area of contact is given by (A.1). The total area of contact per particle is deduced by integrating over all possible initial values of particle–particle spacing

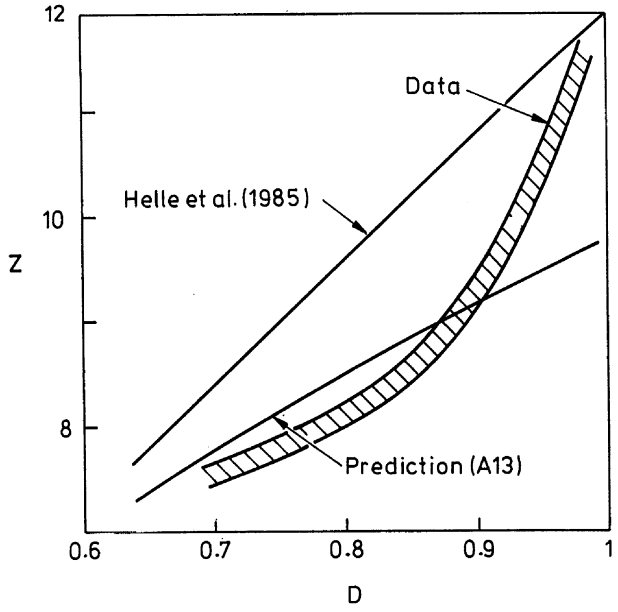

Fig. A2. Number of contacts per particle Z plotted against relative density D, assuming an initial density $D_0 = 0.64$. The predictions (A.13) and that given by Helle *et al.* (1985) are compared with the experimental data of Fischmeister *et al.* (1978). Note that the theoretical predictions are independent of the strain hardening exponent n.

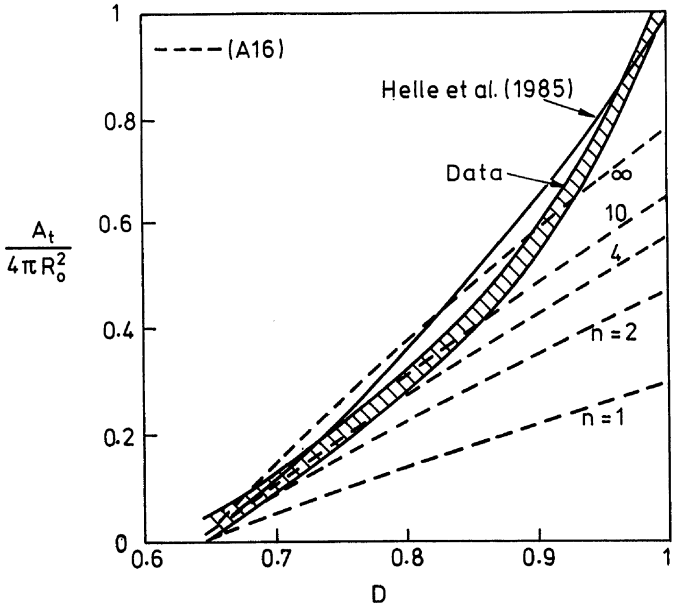

Fig. A3. Total area of contacts A_t normalised by the surface area of a particle $4\pi R_0^2$, plotted against relative density D, for isostatic compaction from an initial relative density $D_0 = 0.64$. The predictions of Helle *et al.* (1985) and the dense random packing calculation (A.16) are compared with the experimental isostatic compaction data of Fischmeister *et al.* (1978), and Kaker and Chaklader (1967). The dependence of the constant c^2 upon strain hardening exponent n in relation (A.16) is taken from Hill *et al.* (1989).

$$A_t = \int_{2R_0}^{2R_0(D/D_0)^{1/3}} \{g(r)A\}\, \mathrm{d}r, \tag{A.14}$$

which gives via (A.1) and (A.3)

$$A_t = 2\pi c^2 R_0^2 Z_0 \left(1 - \left(\frac{D_0}{D}\right)^{1/3}\right) + \pi c^2 R_0^2 C \left(\left(\frac{D}{D_0}\right)^{1/3} + \left(\frac{D_0}{D}\right)^{1/3} - 2\right). \quad \text{(A.15)}$$

Helle *et al.* (1985) suggest that the total contact area per particle is $A_t = ZA_c$, where Z is given by (1.1) and A_c is given by (1.2). The predictions of Helle *et al.* are compared with (A.15) in Fig. A3, along with the experimental isostatic compaction data of Fischmeister *et al.* (1978), and Kaker and Chaklader (1967). We note good agreement between the predictions of (A.15) and the experimental data for realistic values of n in the range 4–10, and D in the range 0.64–0.85. The prediction of Helle *et al.* (1985) lies slightly above both the experimental data and the prediction (A.15) but is acceptable for practical purposes.